Soft Matter

PAPER

View Article Online
View Journal | View Issue

Check for updates

Cite this: *Soft Matter*, 2025, **21**, 1122

Thermotropic reentrant isotropy and induced smectic antiferroelectricity in the ferroelectric nematic realm: comparing RM734 and DIO†

Bingchen Zhong,[a] Min Shuai,[a] Xi Chen,[a] Vikina Martinez,[a] Eva Korblova,[b] Matthew A. Glaser,[a] Joseph E. Maclennan,[a] David M. Walba[b] and Noel A. Clark*[a]

The current intense study of ferroelectric nematic liquid crystals was initiated by the observation of the same ferroelectric nematic phase in two independently discovered organic, rod-shaped, mesogenic compounds, RM734 and DIO. We recently reported that the compound RM734 also exhibits a monotropic, low-temperature, apolar phase having reentrant isotropic symmetry (the I_R phase), the formation of which is facilitated to a remarkable degree by doping with small (below 1%) amounts of the ionic liquid BMIM-PF_6. Here we report similar phenomenology in DIO, showing that this reentrant isotropic behavior is not only a property of RM734 but is rather a more general, material-independent feature of ferroelectric nematic mesogens. We find that the reentrant isotropic phases observed in RM734 and DIO are similar but not identical, adding two new phases to the ferroelectric nematic realm. These phases exhibit similar, strongly peaked, diffuse X-ray scattering in the WAXS range ($1 < q < 2$ Å^{-1}) indicative of a distinctive mode of short-ranged, side-by-side molecular packing. The scattering at small q is, however, quite different in the two materials, with RM734 exhibiting a strong, single, diffuse peak at $q \sim 0.08$ Å^{-1} indicating mesoscale modulation with ~80 Å periodicity, and DIO a sharper diffuse peak at $q \sim 0.27$ Å$^{-1} \sim (2\pi/\text{molecular length})$, with second and third harmonics, indicating that in the reentrant isotropic phase of DIO (which we denote I_R^{lam}), short-ranged molecular positional correlation is smectic layer-like. Both reentrant isotropic phases are metastable, eventually generating birefringent crystals.

Received 22nd August 2024,
Accepted 31st December 2024

DOI: 10.1039/d4sm01008f

rsc.li/soft-matter-journal

Open Access Article. Published on 06 Januar 2025. Downloaded on 09.05.26 05:53:12.
This article is licensed under a Creative Commons Attribution 3.0 Unported Licence.

Introduction

In 2017, two groups independently reported, in addition to the typical nematic (N) phase, novel nematic phases made from strongly dipolar molecules, the "splay nematic" in the molecule RM734[1–3] and a "ferroelectric-like nematic" phase in the molecule DIO.[4] These nematic phases were subsequently demonstrated to be ferroelectric in RM734[5] and in DIO,[6,7] and to be the same phase in these two materials.[7] This phase, the ferroelectric nematic (N_F), is a uniaxially symmetric, spatially homogeneous liquid having nearly saturated polar ordering of its longitudinal molecular dipoles (a polar order parameter > 0.9).[5,8] Chiral doping gives director twist and the second new phase of the ferroelectric nematic realm, the twisted nematic helielectric polarization state (N_F^*).[9–12] DIO also exhibits an antiferroelectric phase, the smectic Z_A (SmZ_A), which has smectic layers of alternating ferroelectric polarization with the director $\boldsymbol{n}$ and polarization $\boldsymbol{P}$ parallel to the smectic layer planes,[13] and several of its close homologs have another new phase, the ferroelectric smectic A (SmA_F), which is also uniaxial but with polarization normal to its smectic layers.[14,15] These novel phases are the gateways to the "ferroelectric nematic realm" of new liquid crystal science.

We recently reported a transition from the ferroelectric nematic liquid crystal (N_F) phase to a low-temperature, liquid phase having reentrant isotropic symmetry (the $I_{R\ phase}$) in mixtures of the liquid crystal compound RM734 with small concentrations of the ionic liquids BMIM-PF_6 (BMIM) or EMIM-TFSI (EMIM), shown in Fig. 1.[16,17] Even a trace amount of ionic liquid dopant was found to facilitate the kinetic pathway of the transition from N_F to I_R, suppressing crystallization and enabling the I_R to form by simple cooling of the N_F. Unlike the N_F, the I_R phase shows no response to applied electric field and thus appears to be nonpolar, *i.e.*, either paraelectric or antiferroelectric, with experiments to date indicating the latter.

[a] *Department of Physics and Soft Materials Research Center, University of Colorado, Boulder, CO 80309, USA. E-mail: noel.clark@colorado.edu*
[b] *Department of Chemistry and Soft Materials Research Center, University of Colorado, Boulder, CO 80309, USA*

† Electronic supplementary information (ESI) available. See DOI: https://doi.org/10.1039/d4sm01008f

This journal is © The Royal Society of Chemistry 2025

Open Access Article. Published on 06 Januar 2025. Downloaded on 09.05.26 05:53:12.
This article is licensed under a Creative Commons Attribution 3.0 Unported Licence.

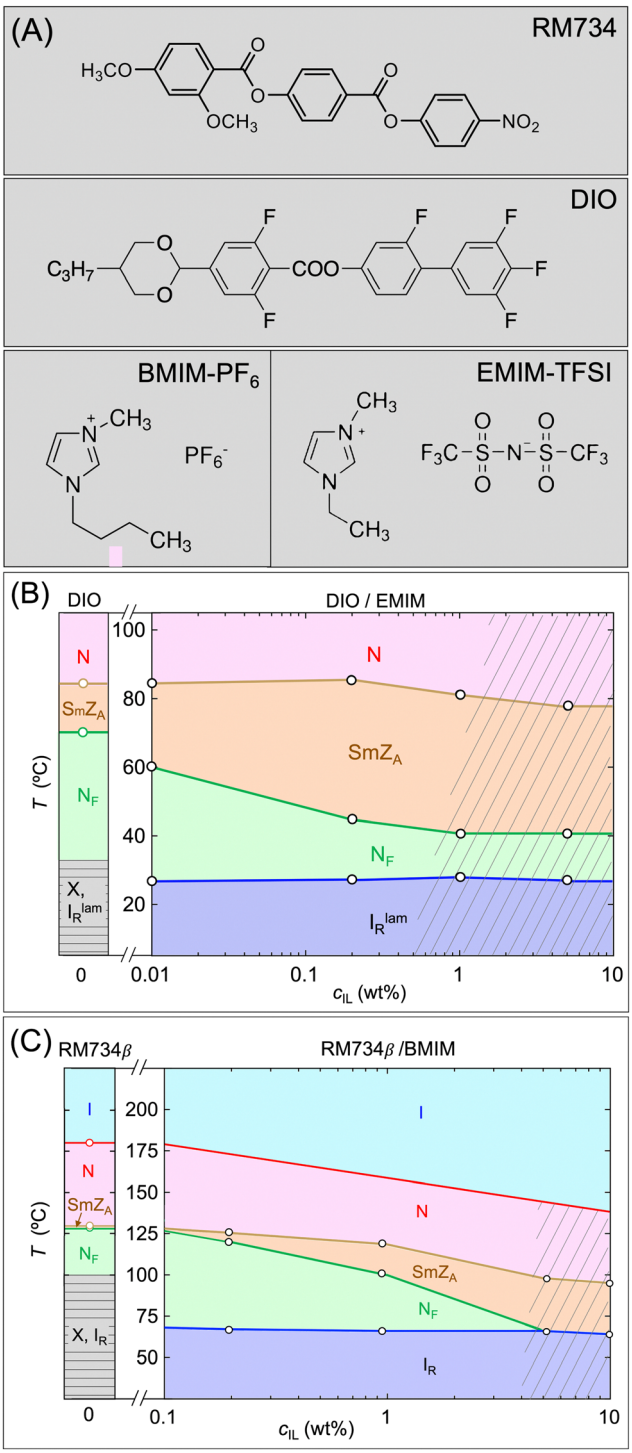

Fig. 1 (A) Structures of the polar mesogens RM734 and DIO and the ionic liquids BMIM and EMIM. (B) Phase diagram of DIO and DIO/EMIM mixtures showing the I_R^{lam}, a new phase of the ferroelectric nematic realm. Pure DIO exhibits the following phase sequence on cooling from 200 °C: high-temperature dielectric isotropic (I); dielectric nematic (N); antiferroelectric smectic Z_A (SmZ_A); ferroelectric nematic (N_F); and, depending on the cooling process, crystal (X) or low-temperature isotropic (I_R^{lam}). The phase diagram of the DIO/EMIM mixtures was determined by X-ray scattering and polarized light microscopy experiments. The times and temperatures required for crystallization were highly dependent on dopant concentration c_{IL} and on sample geometry, with longer times and lower temperatures required as c_{IL} was increased. The shaded region indicates where, at higher dopant concentration, phase separation of EMIM is observed. (C) RM734/BMIM phase diagram for comparison (reprinted with permission from ref. 16). The doped mixtures now both exhibit a modulated, antiferroelectric phase identified as SmZ_A. As in the DIO mixtures, phase separation occurs at higher dopant concentrations (shaded region). Exposing mixtures to temperatures higher than $T \sim 150$ °C produces irreversible changes in phase behavior, so the I–N transition temperature in the mixtures was evaluated only approximately.

The appearance of antiferroelectric ordering adjacent in temperature to the strongly polar-ordered N_F phase may seem surprising but the century-long experimental and theoretical study of ferroelectric materials, both crystals and liquid crystals, shows that ferroelectricity (F) and antiferroelectricity (A) go hand in hand, such that if one is found, the other will also be found in related materials, and that they may even appear as coexisting phases. At the root of this behavior are dipole–dipole interactions and the inherent ambivalence in how dipoles prefer to pack: dipole pairs arranged end-to-end prefer relative parallel orientation and make ferroelectrics, whereas dipole pairs arranged side-by-side prefer relative antiparallel orientation and make antiferroelectrics, differences which are borne out in the basic lattice and Landau models.[18–21] This frustration is almost a recipe for generating modulated, anisotropic, antiferroelectric phases of the SmZ_A type,[14] having ferroelectric stripes of uniform $\boldsymbol{P}$ in the end-to-end direction, and antiferroelectric ordering of adjacent stripes in the side-by-side direction. This richness of new phases and phenomena motivates the notion of a ferroelectric nematic realm, which is further broadened by the report here of the reentrance of isotropic symmetry upon cooling a highly polar and anisotropic N_F liquid crystal state.

Results

We carried out SAXS and WAXS experiments, polarized light microscopy, and polarization current measurement of dilute mixtures of ionic liquid in DIO, focusing here on DIO/EMIM at weight% ionic liquid (IL) concentrations, c_{IL}, in the range ($0\% \leq c_{IL} \leq 5\%$). The molecular species studied are shown in Fig. 1A. These experiments were carried out on a DIO sample synthesized as described in ref. 7, having a phase sequence on cooling I – 173.6 °C – N – 84.5 °C – SmZ_A – 68.8 °C – N_F – 34 °C – X. Our principal results on DIO/IL mixtures, based on X-ray and optical observations, are summarized in the phase diagram of Fig. 1B.

The introduction of IL can produce stunning alterations of phase behavior in mesogens of the ferroelectric nematic realm. Even a very low IL concentration ($c_{IL} \sim 0.01\%$) facilitates the appearance, upon lowering T below ~30 °C, of a new, gel-like bulk phase with reentrant isotropic symmetry (Fig. 1B), which we term the I_R^{lam}, where the subscript R signifies reentrant, distinguishing this phase from that of the usual dielectric isotropic phase (I) found at high temperature, and the superscript "lam" (for "lamellar") distinguishes this isotropic phase from the I_R, the reentrant isotropic phase observed in RM734 (Fig. 1C). Remarkably, even with such low concentrations of IL,

Open Access Article. Published on 06 Januar 2025. Downloaded on 09.05.26 05:53:12.
This article is licensed under a Creative Commons Attribution 3.0 Unported Licence.

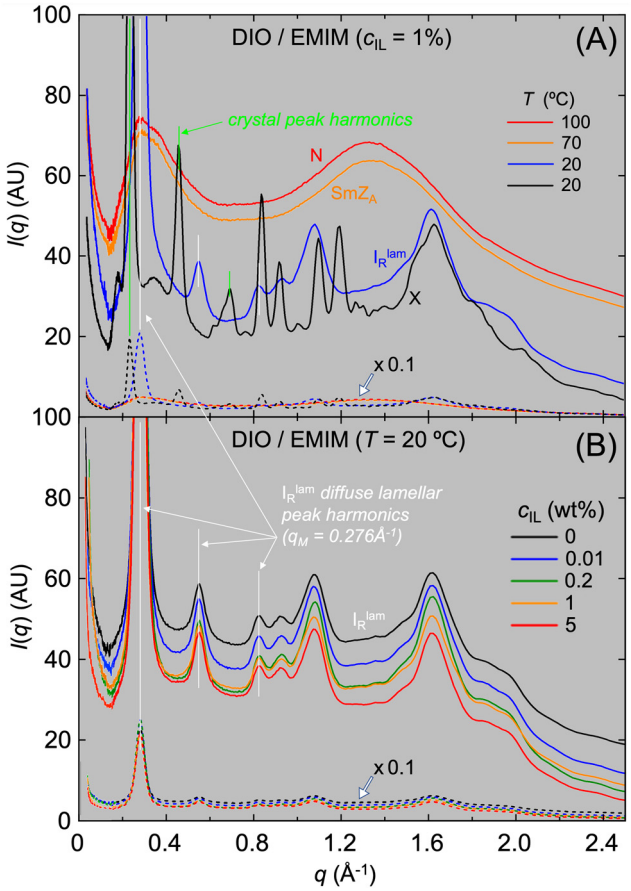

Fig. 2 WAXS scans obtained during slow cooling of DIO/EMIM mixtures. (A) Scans obtained on a c_{IL} = 1wt% DIO/EMIM mixture at selected temperatures show the structure functions $I(q)$ typical of each of the N, SmZ$_A$, I$_R^{lam}$, and X phases. The complete set of scans *vs.* T is shown in the ESI.† The I$_R^{lam}$ phase exhibits a diffuse peak at q_M = 0.2764 Å^{-1} and its first two harmonics (white lines), indicating a lamellar periodicity corresponding to the molecular length of DIO, with end-to-end periodicity $d_M \sim 23$ Å. The distinctive pattern of diffuse peaks in the WAXS q-range indicates side-by side molecular packing which is very different from that of the crystal (X) phase. (B) Scans of the x-ray structure function $I(q)$ of the I$_R^{lam}$ phase *versus* IL concentration c_{IL}. The dependence on c_{IL} is very weak, showing that $I(q)$ of the I$_R^{lam}$ phase is a property of the undoped DIO host. The dashed curves are the solid curves reduced by a factor of 10.

the first-order thermotropic transition upon cooling from the N$_F$ to the I$_R^{lam}$ phase converts the entire sample volume to I$_R^{lam}$, suggesting that the I$_R^{lam}$ phase is intrinsic to the DIO host, with the IL dopant serving to create a kinetic pathway for its nucleation. As in undoped DIO, the SmZ$_A$ phase appears between the N and N$_F$ phases, becoming more stable relative to these phases with increasing IL concentration. The onset of phase separation of the IL component is observed when the dopant concentration $c_{IL} \gtrsim 1\%$ (shaded region). Here we focus on the mesophase behavior at smaller IL concentrations.

In our previous experiments with RM734 as the host,[16] the dopant IL was BMIM. In the present case, the DIO host was doped with EMIM but we have found that BMIM and EMIM behave very similarly in both materials, with both ILs facilitating the kinetic pathway to a reentrant isotropic phase, the structure of which is a property of the host N$_F$ and does not depend on the IL concentration (see Fig. 2B, C and Fig. 2B of ref. 16) or on which ionic dopant is used (see Fig. 7 of ref. 16).

X-ray scattering

Powder-average SAXS and WAXS scans of temperature-controlled samples in 0.7 mm to 1 mm diameter thin-wall capillaries were obtained during slow cooling, with results shown in Fig. 2 and 4–6.

Temperature dependence with c_{IL} = 1%

A selection of X-ray scans at temperatures in the N, SmZ$_A$, N$_F$, I$_R^{lam}$, and X phases in the c_{IL} = 1% mixture are shown in Fig. 2A. Complete cooling sequences for this and the other c_{IL} values are provided in the ESI.† The higher-temperature, anisotropic, N, SmZ$_A$, and N$_F$ phases each exhibit a broad, diffuse WAXS peak at $q \sim 1.5$ Å^{-1}, the powder average of the equatorial diffuse peak observed in the WAXS of magnetic field-aligned N and N$_F$ DIO samples due to the side-by-side positional correlation arising from steric repulsion of the molecules.[1,7] The transition to the I$_R^{lam}$ phase is marked by significant changes in this scattering, with the broad WAXS peak breaking up into several much narrower diffuse peaks with scattering wavevectors q in the range (0.8 Å^{-1} < q < 2.2 Å^{-1}), marking the development of specific, longer-ranged, side-by-side intermolecular positional correlations in the I$_R^{lam}$ phase.

Dopant concentration dependence at T = 20 °C

The X-ray scattering $I(q)$ of the I$_R^{lam}$ phase at T = 20 °C at several different concentrations, c_{IL}, of EMIM in DIO is shown in Fig. 2B. It is evident from these scans that the structure of the X-ray peaks in the I$_R^{lam}$ phase varies only very weakly with concentration for c_{IL} in the range (0.01% ≤ c_{IL} ≤ 5%), in both the SAXS and WAXS regimes. This, and the fact that the I$_R^{lam}$ phase is observed at very low dopant concentrations, suggests that the causative molecular organization of the I$_R^{lam}$ phase is intrinsic to the DIO host.

Comparison of reentrant isotropic scattering of DIO with that of RM734

The reentrant isotropic structure functions $I(q)$ of pure RM734 and DIO at T = 20 °C are compared directly in Fig. 3. Remarkably, the WAXS scattering of the I$_R^{lam}$ phase of DIO bears a strong resemblance to that observed in the I$_R$ phase of RM734, with two prominent diffuse peaks in each scan, a similarity that suggests that the existence of the I$_R$ is a general phenomenon of ferroelectric nematic mesogens, and not just a peculiarity of RM734. The scattering at shorter wavevectors ($q \lesssim 0.8$ Å^{-1}) in the two materials is, however, quite different. The single, small-angle diffuse peak of RM734 is located at $q_M \approx 0.080$ Å^{-1} but DIO exhibits a sequence of three, narrower, diffuse peaks, at $q_M \approx 0.27$, 0.55, and 0.83 Å^{-1}, a 1:2:3 harmonic series indicating strong local lamellar order with a layer spacing $d_M \sim 23$ Å, approximately the molecular length of DIO. The fundamental is at the same wavevector as the strong, diffuse scattering feature along $\boldsymbol{q}_z$, where z is parallel to the director, observed in all of the LC phases of DIO[7,13] and close to that of

 This journal is © The Royal Society of Chemistry 2025

Open Access Article. Published on 06 Januar 2025. Downloaded on 09.05.26 05:53:12.
This article is licensed under a Creative Commons Attribution 3.0 Unported Licence.

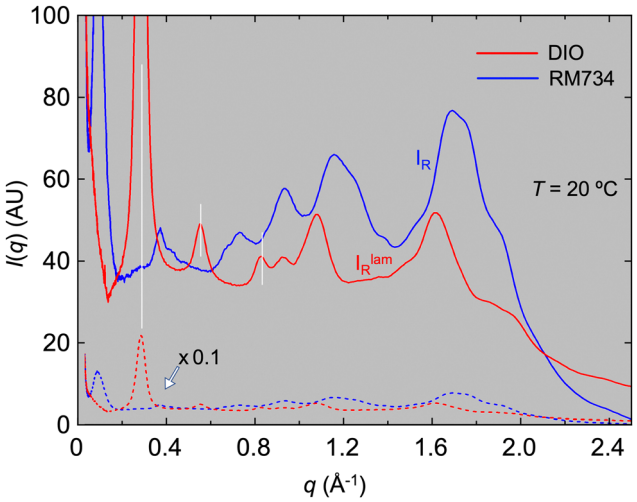

Fig. 3 Comparison of X-ray diffraction scans of the reentrant isotropic phases of pure DIO and RM734. The I_R^{lam} phase of DIO exhibits a series of three diffuse peaks at q_M = 0.2764 Å^{-1} and its first two harmonics (white lines), indicating a lamellar periodicity corresponding to the DIO molecular length (hence the name I_R^{lam}), and a distinctive pattern of diffuse peaks in the WAXS q-range from side-by-side molecular packing. The scattering from the I_R phase of RM734 is similar in appearance but does not show any harmonics. As shown in Fig. 2B of ref. 16, and in Fig. 2B above, the form of the scattering of the reentrant isotropic phases in RM734 and in DIO does not depend significantly on ionic dopant concentration.

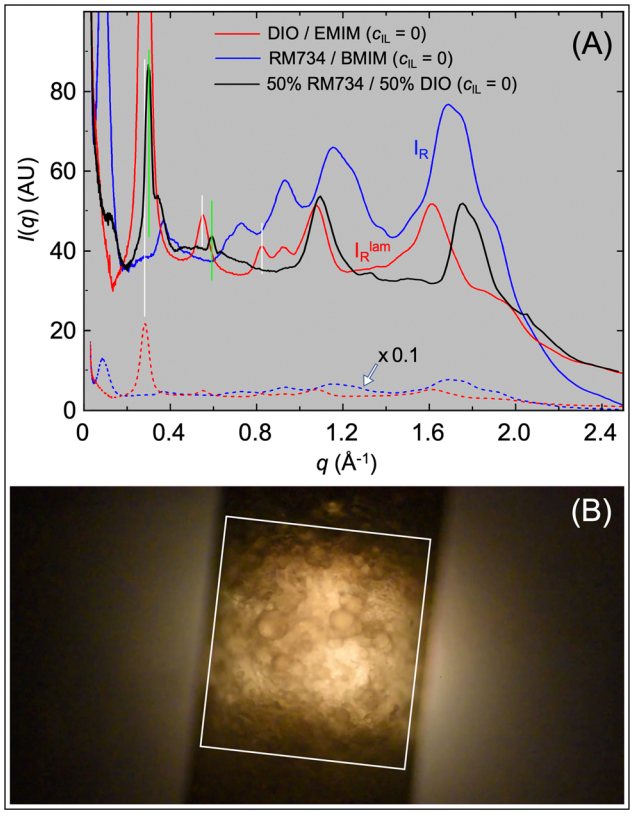

Fig. 4 (A) Comparison of X-ray diffraction scans of the reentrant isotropic phases of: DIO/EMIM (c_{IL} = 0, red) and RM734/BMIM (c_{IL} = 0, blue) with 50% RM734/50% DIO (c_{IL} = 0, black). The X-ray scattering from the reentrant isotropic phases in the 50/50 mixture exhibits the principal features of those of the scans of doped RM734 and DIO, but with the following notable differences: (i) prominent WAXS peaks similar to those observed in the individual doped materials are present in the 50/50 mixture but the peak positions and structures are not describable as superpositions of the RM734 and DIO WAXS peaks. Also, the peak corresponding to small-q, lamellar scattering in doped DIO is shifted in wavevector from q_M = 0.276 Å^{-1} to 0.297 Å^{-1} in the 50/50 mixture. (ii) the SAXS peaks of doped RM734 and DIO are also present in the 50/50 mixture, but at much lower intensity relative to the WAXS than in the RM734 and DIO scans, reduced by factors of between five and ten, as seen by comparing the solid black curve with the red and blue ones. These differences indicate that each of the coexisting reentrant isotropic phases in the 50/50 mixture has a substantial minority fraction in its composition. The local molecular packing thus appears to be maintained in the coexisting phases, but at larger length scales the ordering is disrupted. (B) Transmitted light image of a 50%RM734/50% DIO mixture in a 0.7 mm diameter X-ray capillary cooled from the N phase to 50 °C, showing the phase separation of RM734- and DIO-rich globules, as well as the X-ray beam dimensions (white square). These globular domains are maintained respectively as distinct I_R and I_R^{lam} phases at room temperature.

the smectic A_F phase observed in binary mixtures of DIO with the mesogen 2N,[14] and of close molecular analogs of DIO.[15,22] Thus, the tendency of DIO to form locally layered structures with molecular monolayer spacing is also manifest in its reentrant isotropic phase as short-ranged, molecular-monolayer lamellar ordering. We consequently term the reentrant isotropic in DIO the I_R^{lam} phase.

50% RM734/50% DIO

In order to further explore reentrant isotropy as a phenomenon of the ferroelectric nematic realm, we studied the reentrant isotropic phase behavior of a 50% RM734/50% DIO mixture, with results shown in Fig. 4. Optical microscopy of capillaries of this mixture, shown in Fig. 4B, shows an I_R phase growing in, coexisting with the N_F phase. A key observation is that, like the I_R phase of RM734 (Fig. S1 (ESI†) in ref. 17), this reentrant isotropic appears as dynamic fluid blobs growing in diameter and coalescing, showing definitively that, like the I_R phase of RM734, this phase is fluid. At lower temperature, a second isotropic phase grows in, giving coexisting reentrant isotropic domains in the capillary. X-ray scattering of a sample volume containing many dispersed droplets of one phase in the other exhibits the principal features of the individual RM734 and DIO scans in Fig. 3 but cannot be modeled as a linear combination of them (recalling that $I(q)$ of the reentrant isotropic in both doped RM734 and doped DIO does not depend strongly on c_{IL}). Specifically: (i) the main peaks in the WAXS region are of comparable width and intensity to those of RM734 and DIO but are at different q-values; (ii) the DIO-like SAXS peaks are weaker relative to the WAXS peaks for both the RM734 and DIO contributions to the black curve in Fig. 4A; (iii) the peak corresponding to small-q lamellar scattering in doped DIO is shifted in wavevector from a fundamental wavevector q_M = 0.276 Å^{-1} (white lines) to q_M =0.297 Å^{-1} (green lines) in the 50/50 mixture (Fig. 4A); (iv) the diffuse SAXS peak similar to that in RM734 is at q_M = 0.125 Å^{-1}. These differences indicate that each of the coexisting reentrant isotropic phases in the 50/50 mixture must have some minority fraction of either RM734 or DIO in its individual composition.

Open Access Article. Published on 06 Januar 2025. Downloaded on 09.05.26 05:53:12.
This article is licensed under a Creative Commons Attribution 3.0 Unported Licence.

Optical textures and electro-optics of DIO/EMIM mixtures

Polarized light microscopy observations of the mixtures were made in cells with the LC between a pair of glass plates spaced 3.5 μm apart. One plate was coated with a pair of ITO electrodes separated by a 1.04 mm wide gap used to apply an electric field, E, largely parallel to the sample plane. These cells were filled and studied only at temperatures below 120 °C, as the components thermally degraded at higher temperatures, resulting in irreversible changes in phase behavior. The plates were treated with polyimide layers with antiparallel buffing along a direction 3° from being parallel to the electrode edges. In the N phase, this preparation produces uniform, planar alignment of the director $\boldsymbol{n}(\boldsymbol{r})$, the local mean molecular long-axis and the optic axis, parallel to the glass and 3° from normal to the field. Upon cooling into the N_F phase, the $\boldsymbol{n}(\boldsymbol{r})$–$\boldsymbol{P}(\boldsymbol{r})$ couple transitions to a π-twisted geometry, a result of the antiparallel orientation of the ferroelectric polarization, $\boldsymbol{P}(\boldsymbol{r})$, on the two surfaces, as previously detailed.[8] The angular offset of the rubbing direction ensures a well-defined initial reorientation direction of $\boldsymbol{n}(\boldsymbol{r})$ with application of a given sign of electric field.

Cooling a c_{IL} = 0.2% DIO/EMIM mixture from the N to the N_F phase at T = 30 °C results in the formation of uniformly twisted N_F domains, shown in Fig. 5A. In contrast to pure DIO, where the walls observed between π-twisted domains of opposite handedness have a characteristic faceted shape, a morphology that is a compromise between the polarization charge deposited at the wall and the wall length,[9] the domain walls in the presence of ionic liquid dopant become smooth, a consequence of polarization charge screening at the domain boundaries. Further cooling induces the N_F to I_R^{lam} phase transition at $T \approx$ 27 °C, where small, extinguishing I_R^{lam} domains nucleate *via* a first-order transition, as seen in Fig. 5B. These I_R^{lam} domains, which are dark between crossed polarizer and analyzer at all sample orientations, eventually grow to cover the entire sample area (Fig. 5C). The extinction of the final I_R^{lam} dark state between crossed polarizers is comparable to that of the high temperature I phase. In all cells, and at all c_{IL} concentrations, we observe a patchy texture of weakly transmitting areas of low remnant birefringence, apparently due to sub-10 nm thick birefringent layers on the glass surfaces in which there may be induced nematic order. Application of in-plane electric fields of a few V mm^{-1} that easily reorient the bulk director/polarization couple in the N_F phase to be nearly along the field[5] has no visible effect on the dark I_R^{lam} domains, suggesting that the I_R^{lam} structure is apolar. Squeezing the cells and manipulation of free drops show that macroscopically the I_R^{lam} phase is a viscoelastic liquid.

SmZ_A phase

Undoped DIO exhibits a phase between the N and N_F, the smectic Z_A, which we have shown previously to be lamellar, having an antiferroelectric array of layers with the polarization parallel to the layer planes.[13] The SmZ_A layering in undoped DIO appears in X-ray diffraction as very weak peaks in the SAXS range which to date have required a synchrotron source to

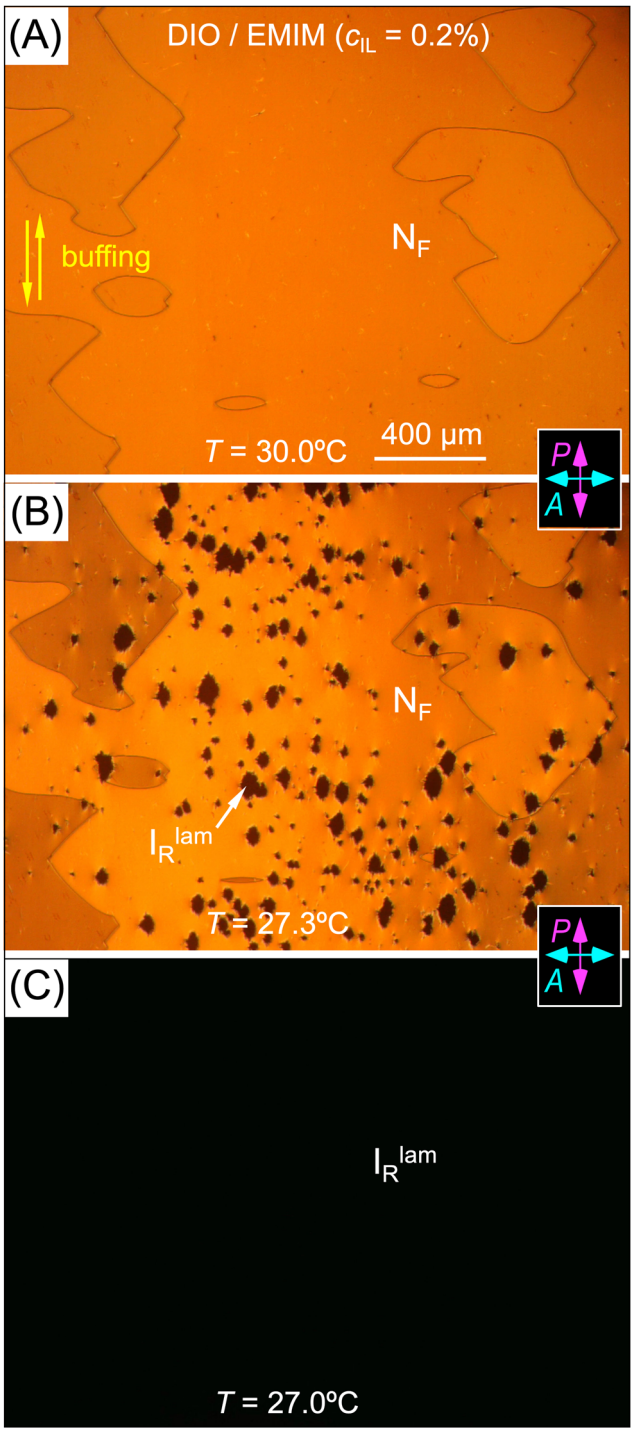

Fig. 5 (A) Polarized light microscopy image of a 3.5 μm thick DIO/EMIM (c_{IL} = 0.2%) mixture in the N_F phase between glass plates with antiparallel-rubbed alignment layers. This surface treatment imposes a director structure in the N_F phase that is uniformly twisted by π from one plate to the other,[8] producing an orange birefringence color between crossed polarizer and analyzer. Domains with twist of opposite handedness have slightly different hues. (B, C) Following continuous slow cooling, at around 27 °C, dark, optically isotropic domains of the I_R^{lam} phase nucleate and grow, eventually covering the entire cell area. At low temperatures, the I_R^{lam} region has an extinction coefficient comparable to that of the high-temperature isotropic phase, and of air bubbles in the same cell.[16]

This journal is © The Royal Society of Chemistry 2025

Open Access Article. Published on 06 Januar 2025. Downloaded on 09.05.26 05:53:12.
This article is licensed under a Creative Commons Attribution 3.0 Unported Licence.

observe.[13,14] Otherwise, the X-ray scattering from the SmZ_A in the SAXS/WAXS ranges obtained using our in-house diffractometer does not differ substantially from that of its neighboring N and N_F phases, so is not useful for phase identification. However, the lamellar nature of the SmZ_A phase is also manifest in a host of characteristic textural features previously observed in the study of smectics, which, on their own, enabled identification of this intermediate phase as a smectic in undoped DIO, using the cell geometries and characterization methods, including electric field application and temperature scanning, described in ref. 13.

The same experimental methods were applied to the DIO/EMIM mixtures, leading to the phase diagram of Fig. 1, in which the phase between N and N_F is identified as SmZ_A. As noted, the X-ray scattering from this phase in the doped sample, exemplified for c_{IL} = 1% in Fig. 2A, is quite similar to that of its neighboring N and N_F phases. However, the visual signatures of the SmZ_A layer ordering in the cell textures are quite unmistakable across the concentration range shown in Fig. 1. An example of this is shown in Fig. 6, in which comparable arrays of zig-zag smectic layering defects are shown in c_{IL} = 0 and c_{IL} = 1% DIO/EMIM samples. This requires nearly identical birefringence, the same alignment of $\boldsymbol{n}$ parallel to the buffing, the same alignment of layer normal $\boldsymbol{q}_M$ nearly parallel to the plates, and the same layer organization within the zig-zag walls, defects that mediate reversal of the smectic layer chevron direction. Similarities such as these lead to the identification of this intermediate phase in DIO/EMIM mixtures as SmZ_A.

Significantly, as indicated in Fig. 1, while undoped RM734 has no SmZ_A phase, the addition of a small amount of IL dopant (c_{IL} = 1%) is sufficient to induce a 20 °C-wide, SmZ_A-like phase between the N and N_F phases. This phase is antiferroelectric, has the layer normal $\boldsymbol{q}_M$ oriented perpendicular to the director $\boldsymbol{n}$, and exhibits zig-zag walls as shown in Fig. 5 of ref. 16, all characteristic features of the smectic Z_A phase but with layers that are several μm thick, much larger than the 8 nm layer spacing of the SmZ_A phase in DIO.

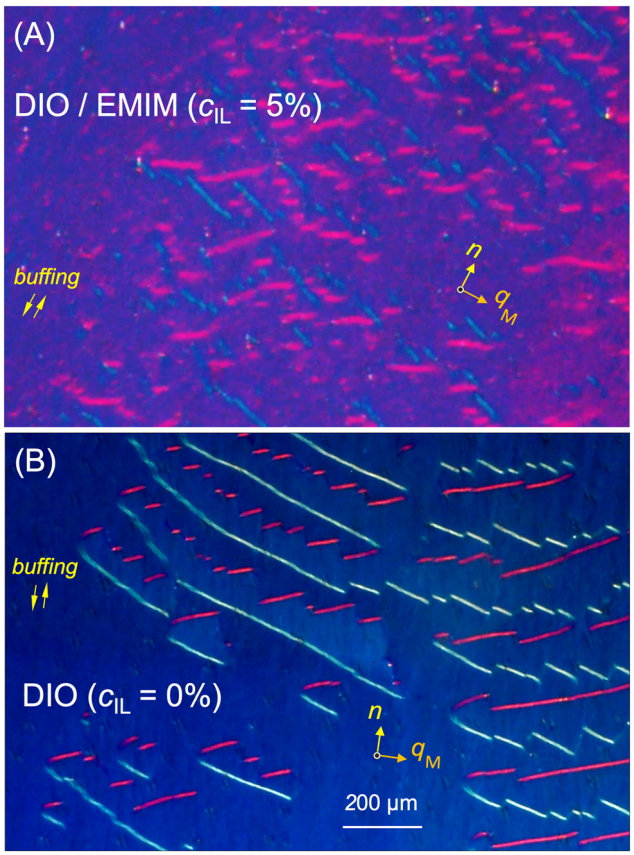

Fig. 6 Comparison of the textures of the modulated phase intermediate between the N and N_F phases in a DIO/EMIM mixture and of the SmZ_A phase in a pure DIO sample: (A) DIO/EMIM (c_{IL} = 1%) mixture; (B) undoped DIO (c_{IL} = 0%). The samples are contained in d = 3.5 μm cells that have antiparallel-buffed, polyimide-coated plates. The phases exhibit very similar characteristics: comparable birefringence; alignment of $\boldsymbol{n}$ parallel to the buffing; layer normal orientation $\boldsymbol{q}_M$ nearly parallel to the bounding plates; and chevron-layering reversal defects (zig-zag walls) (cyan and magenta in these images). When such lamellar phases are confined between flat plates with the layers normal to the plates (bookshelf alignment), it has been found that when the sample temperature is changed in such a way that the layers shrink (heating the SmZ_A, in the present case), the layers will buckle in an effort to maintain the bookshelf pitch along the average layer normal direction,[23] resulting in chevron layer structures[24] and, on a larger scale, zig-zag walls.[25] These similarities lead to the identification of this intermediate phase in DIO/EMIM mixtures as SmZ_A. Detailed discussion of the zig-zag wall structure can also be found in Fig. 4 of ref. 13. (B) is reprinted from ref. 13 with permission.

Discussion

The notion of the "ferroelectric nematic realm" as a field of activity and interest in LCs was motivated by our observation of the ideal binary miscibility of RM734 and DIO in the ferroelectric nematic (N_F) phase.[7] These two molecular species exhibit the same ferroelectric nematic phase and possess some required but yet to be definitively identified commonality that enables them to behave as equivalent participants in an N_F fluid mixture. This transforms N_F fluid formation into a mechanism of selection, which, given the late date of discovery of the N_F, is apparently rare among mesogens. In the case of the N_F, this selection has led, remarkably, to the observation of other new phases like the chiral N_F,[9] the smectic Z_A,[13] and the smectic A_F,[14] which are related to the N_F by having polar ordering of similar magnitude on some length scale.

These connections define the ferroelectric nematic realm, a field which is significantly enriched and enhanced by the results presented here: the surprising appearance of reentrant isotropy in RM734[16] is now found to be a trick that DIO also performs, albeit with its own twist. The N_F phase, with its saturated quadrupolar order parameter and nearly perfect polar order even at elevated temperature, can perhaps be considered the most-ordered nematic phase, combining nearly perfect, long-range polar orientational order and short-range positional disorder. The I_R-type reentrant isotropic phases appear to be an exchange of this N_F state for one having exceptionally robust, apolar, short-range molecular positional correlations (Fig. 2A) that stabilize a macroscopic, transparent, optically isotropic, homogeneous phase. The thermodynamic availability of the

Open Access Article. Published on 06 Januar 2025. Downloaded on 09.05.26 05:53:12.
This article is licensed under a Creative Commons Attribution 3.0 Unported Licence.

I_R-type phases upon cooling points to internal energetic frustration in the N_F as the principal driving force for this transition.

The position of the peak at smallest angle in DIO ($2\pi/q_M$ = $d_M \approx 23$ Å) is indicative of local monolayer lamellar electron-density modulation which, given the isotropy and transparency of the I_R^{lam} observed optically, would be some form of short-ranged smectic A_F ordering.[14] However, this peak is diffuse, Scherrer broadened to a half-width at half-maximum (HWHM) $\delta q \sim 0.023$ Å^{-1}, indicating an exponential decay of layer coherence with a characteristic distance of $\sim$42 Å, *i.e.*, local structures of just a few layers. The lack of dependence of the I_R^{lam} x-ray peak structure on ionic dopant concentration seen in Fig. 2B, in both the SAXS and WAXS wavevector regimes, indicates that the causative molecular organization of the I_R^{lam} phase is predominantly a property of the DIO host.

In an effort to gain insight into the local structure of the I_R^{lam} phase, we made a broad study of the prior art of systems which can be considered relevant, *i.e.*, those that share with the I_R^{lam} most of the following features: being thermotropic and having few-components; comprised of rod-shaped molecules or molecular segments; having short-range smectic local ordering, an optically isotropic phase in addition to the high temperature one, and the higher-q scattering features coming from side-by-side correlations of rod-shaped molecular segments.

Prior art

Thermotropic liquid crystal reentrant isotropy was first reported by Luzatti and Spegt in the cubic *Ia3d* gyroid phase of strontium alkanoates,[26,27] a phase structure which was also found in the phenyl carboxylate dimers NO_2-*n*-BCA upon cooling from a smectic C,[28–30] and has been observed since then in numerous other systems.[31–34] The local gyroid structure is an assembly of molecules into extended supermolecular linear aggregates which form three interlinked sets of spring-like helices, one set running along each of the cartesian coordinate directions to generate a lattice of cubic symmetry made up of mesoscopic unit cells containing hundreds to thousands of molecules.[26–34] Their cubic symmetry renders such phases optically isotropic. The gyroid helices are chiral, which opens the possibility of isotropic phases having macroscopic chirality and consequent optical activity, even if the constituent molecules are achiral. Achiral molecules can also give rise to achiral isotropic phases if helical segments are found in mirror-symmetric pairs, as in the *Ia3d*.

Another specific example, which may be of particular relevance to the I_R phase, is the fluid isotropic cubic phase obtained upon cooling the smectic C in the 1,2-bis(4′*n*-alkoxybenzoyl) hydrazine (BABH-*n*) homologous series, also *Ia3d*.[35–43] In this system, at low temperatures the intermolecular hydrogen-bonding between side-by-side, rod-shaped cores enhances the hourglass shape of the molecules (thin cores with fat tails), and thereby the tendency for local twist, stabilizing a cubic phase having equivalent helical networks of opposite chirality.[44] Heating increases the side-by-side entropic repulsion of the flexible tails, breaking the intermolecular hydrogen bonds and producing a smectic C phase. Such effects of tail entropy can be enhanced by the use of multi-tail (phasmidic) molecules, making induction of local twist an effective method for obtaining cubic phases.[32,33,45]

Extensive X-ray scattering on powder samples has been carried out on such cubic soft crystal systems in the low-Miller index range of their cubic lattice reciprocal spaces, generally with scattering vectors in the SAXS regime ($q \lesssim 0.4$ Å^{-1}). In many such cases, sets of scattering peaks can be indexed, and in some cases the peak intensities have been used to calculate unit cell electron density. The observed peak widths appear to be broader than the resolution limits, indicating that crystallite sizes, deduced from the inverse X-ray peak widths, are limited by lattice defects. However, optical observations show the growth of millimeter-dimension, cubic single crystals in some systems,[32] providing direct evidence for long-range cubic crystal order.

In contrast, the SAXS scattering from the reentrant isotropic phases of DIO and RM734 show no long range-positional ordering. DIO exhibits a sequence of three diffuse peaks, at $q \approx 0.27$, 0.55, and 0.83 Å^{-1}, a 1 : 2 : 3 harmonic series indicating strong local lamellar order with a layer spacing $d_M \sim 23$ Å, approximately the molecular length of DIO. The fundamental is at the same wavevector as the strong, diffuse scattering feature along $\boldsymbol{q}_z$, where $\boldsymbol{z}$ is parallel to the director, observed in all of the LC phases of DIO[7,13] and close to that of the smectic A_F phase observed in binary mixtures of DIO with the mesogen 2N,[14] and of close molecular analogs of DIO.[15,22] Thus, the tendency of DIO to form local smectic layering structures with molecular monolayer spacing is also manifest in its I_R^{lam} phase as short-ranged, molecular monolayer lamellar ordering.

The SAXS scattering from the reentrant isotropic phase of RM734 differs from that of DIO, exhibiting a single peak at scattering vectors in the range 0.07 Å$^{-1} \lesssim q(T) \lesssim 0.1$ Å^{-1}, with a HWHM $\delta q \sim 0.03$ Å^{-1} that is two orders of magnitude broader than the diffractometer resolution. Thus, this RM734 SAXS scattering peak is diffuse, indicating short-range positional correlations which, given this $q(T)$ range, have a length scale comparable to the unit cell sizes in the cubic systems cited above but without long-range cubic crystalline order.

The DIO short-range order qualitatively fits the picture of the "sponge phases" of lyotropic amphiphiles,[46] and bent-core smectics,[47] and of the Cubic*(*Ia3d*) – Iso_1* – Iso_2 phase sequences with increasing temperature observed by Tschierske and coworkers in a family of achiral polycantenar mesogens, which exhibit *Ia3d* cubic phases with macroscopic spontaneous chirality.[48,49] The Iso_1* phase has a diffuse scattering peak at q-values where the cubic phase of this family has Bragg reflections, indicating short-range, cubic positional correlations. Remarkably, such correlations can maintain the macroscopic chirality of the cubic lattices, the Iso_1* exhibiting conglomerate domains of opposite optical rotation, indicating that they preserve and transmit their local chiral structure to their neighbors[48,49] even in the absence of a long-range lattice, as has also been found in bent-cores.[47] The I_R phase of RM734 may be an achiral example of such behavior, exhibiting similar cubic correlations, suggesting that a related, lower-temperature phase with long-range, cubic structure may exist.

Importantly, while the SAXS data on cubic phases is extensive, there have been very few systematic studies of reentrant

 This journal is © The Royal Society of Chemistry 2025

Open Access Article. Published on 06 Januar 2025. Downloaded on 09.05.26 05:53:12.
This article is licensed under a Creative Commons Attribution 3.0 Unported Licence.

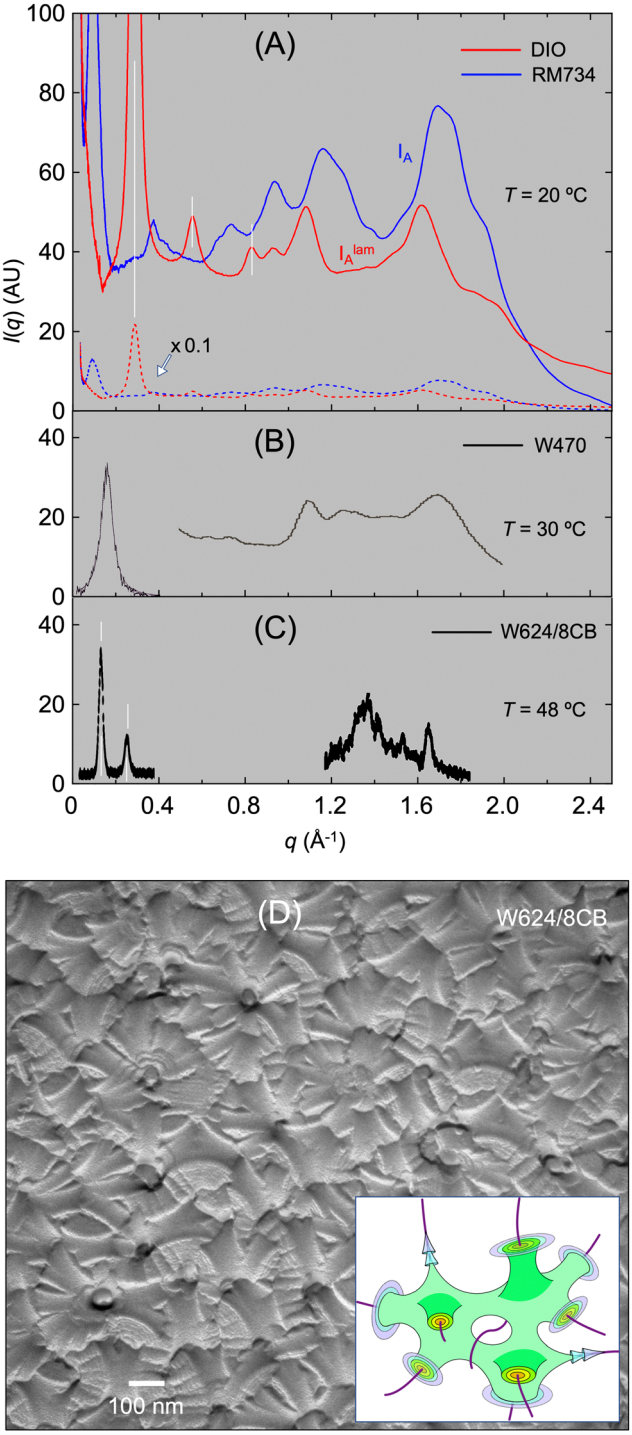

Fig. 7 Comparison of x-ray diffraction from the reentrant isotropic phases of RM734 and DIO with the scattering from other mesogenic systems that exhibit a reentrant isotropic phase and have similar X-ray diffraction signatures. (A) Full X-ray scans (SAXS + WAXS) of the I_R phase in RM734 and the I_R^{lam} phase in DIO, with the diffuse lamellar peaks in DIO indicated by white lines. (B) SAXS + WAXS scans of the reentrant isotropic phase of the single-component, chiral calamitic mesogen W470, from ref. 53. The molecule gelates when dissolved, forming networks of nanoscale filaments, but the structure of the reentrant isotropic phase has not been visualized. (C) SAXS + WAXS scans of the reentrant isotropic phase of a 50/50 mixture of the bent-core mesogen W624 and 8CB. The white lines indicating the SAXS diffuse peak wavevectors are at q-values with the ratio 1 : 2, indicating that the local structure is lamellar (smectic-like), as in DIO. (D) FFTEM image of the local structure of the reentrant isotropic phase of W624/8CB, showing a network of nested smectic cylinders which form a disordered array of multiply connected filaments (locally a gyroid sponge phase). This is a possible model of the DIO I_R^{lam} phase structure. The data in (B) are reproduced from ref. 53 with permission. The data in (C) and (D) are reproduced from ref. 51 with permission.

isotropics in the WAXS range ($q > 0.5$ Å^{-1}), where larger scattering vectors can probe the details of molecular side-by-side packing, of relevance in our system. High-temperature phases such as the spontaneously chiral cubics have a broad, diffuse WAXS reflection,[48] similar to that of the high-temperature N and N_F phases of RM734.

However, we have found several experimental systems which exhibit low-temperature, isotropic polymorphism and have distinct, diffuse WAXS peaks very similar to those of the I_R phase, the first being the 50 wt% mixture of the rod-shaped mesogen 8CB with the material W624 (compound **2b** in ref. 50), where a thermotropic Smectic C – to – Isotropic* dimorphism was observed.[51] X-ray scattering (Fig. 7C) and extensive FFTEM visualization of the local structure (Fig. 7D) in the spontaneously chiral Isotropic* (dark conglomerate) phase[51] showed it to be lamellar with strong side-by-side molecular positional correlations, its X-ray scattering bearing a strong resemblance to that of DIO and RM734 shown in Fig. 7A, and having a strong tendency for local saddle-splay layer curvature (see Fig. 7D), the latter driving the assembly of gyroid-like, branched arrays of filaments of nested cylindrical layers. A similar low-temperature isotropic phase was found also in the single-component bent-core molecule 12-OPIMB.[51] The local nested-cylinder layer structure of these phases, exemplified in the W624/8CB mixture, features director splay everywhere, a mechanism which has also been proposed to stabilize phases in the ferroelectric nematic realm.[2,52] A third, quite different low-temperature isotropic system that gives X-ray scattering more like the I_R^{lam} phase of DIO shown in Fig. 7B is that of a small, azo-based molecule (W470), which has a chiral smectic C phase between a high-temperature isotropic phase and a low-temperature reentrant isotropic phase, with FFTEM showing the latter to form side-by-side, linear aggregates and gels when diluted with solvent.[53] However, the bulk structure of the reentrant isotropic phase of neat W470 has not been established.

The soft cubic phases discussed above are based on nanosegregation, which in the gyroid case involves the formation of filamentous networks. Other nanosegregation motifs which may be relevant to understanding the I_R phase are the formation of localized aggregates, such as micelles or localized topological singularities, which then self-assemble into higher-symmetry arrays.[26] Experimental demonstrations include crystals of complex defects such as skyrmions[54] and knots,[55] block-copolymers,[56] and hybrid thermotropic 3D variations, the so-called "transparent nematic" in which dispersed didodecylammonium bromide micelles serve as the cores of fluid hedgehog defects in a rod-shaped mesogenic nematic.[57,58] Periodic arrays of nematic topological defects have been shown theoretically to form stable, space-filling crystal structures.[44,59–62]

Open Access Article. Published on 06 Januar 2025. Downloaded on 09.05.26 05:53:12.
This article is licensed under a Creative Commons Attribution 3.0 Unported Licence.

The N_F state is a phenomenon of the ferroelectric nematic realm – there are many structural variants of RM734 and DIO and other molecules that include a few specific required features (currently not completely understood) which enable them to be ferroelectric nematic. Molecular pairs of the realm are broadly miscible in the N_F phase. RM734 and DIO, for example, make ideal mixtures in the N_F phase, indicating that they are interchangeable on a single-molecule basis in the nature of their participation in the generic N_F ordering. It appears from this work and that of ref. 17 that transitioning into a reentrant isotropic phase is also a generic consequence of the aforementioned specific features.

In ionic liquids there are attractive positional correlations between the anions and cations.[63] In ferroelectric nematics, the dominant molecular correlation is electrostatically stabilized, chain-like polar end-to-end association,[5] where such chains when side-by-side tend also to polar order. It may be that ± IL pairs can complex with the polar molecules to rather lock in antiparallel order or break up the chains in some way. Whatever the mechanism, it must interface in a direct way with that of the N_F ordering itself. A simple manifestation of this may be frustration, for example the N_F polar ordering mechanism enthalpically generating polar ordering that is ''too good'', and subject to escape mechanisms that can raise the entropy. In any case, understanding the reentrant isotropic phenomenon will go a long way toward truly understanding the origin of the N_F state.

Conclusions

In summary, we have demonstrated that the prototype ferroelectric nematic compound DIO exhibits a low-temperature, apolar, reentrant isotropic phase similar to that recently reported in RM734. The formation of this phase is facilitated by doping with small amounts of the ionic liquid EMIM-TFSI. X-ray scattering from the reentrant isotropic phase of DIO shows multiple, narrow, diffuse peaks resembling those seen in the reentrant isotropic phase of RM734, indicating specific, short range, intermolecular positional correlations on the scale of a few nanometers. In contrast to RM734, though, DIO also shows three harmonic peaks, indicating strong local lamellar order with a layer spacing close to the molecular length of DIO. We therefore term the reentrant isotropic phase in DIO the I_R^{lam} phase. Observation of reentrant isotropy in these two distinct molecular species indicates that this is a generic feature of the ferrolectric nematic realm.

Materials and methods

The mixtures were studied using standard liquid crystal phase analysis techniques previously described,[5,7,8] including polarized light microscopic observation of LC textures and response to electric field, X-ray scattering (SAXS and WAXS), and techniques for measuring polarization and determining electro-optic response.

Materials

DIO was synthesized by the Walba group as described in[13] (DIO phase sequence: I – 173.6 °C – N – 84.5 °C – SmZ_A – 68.8 °C – N_F – 34 °C – X). EMIM-TFSI {1-Ethyl-3-methylimidazolium bis(trifluoromethylsulfonyl)imide} was obtained from Millipore/Sigma and used without further purification.

Methods – obtaining the I_R^{lam} phase in undoped DIO or DIO/IL mixtures

Samples of DIO and its mixtures with ionic liquid were heated into the N phase at 120 °C before they were loaded into capillaries or liquid crystal cells. After filling, the X-ray capillaries were quenched on a flat metal surface at $T = -19$ °C, by which means the entire volume of the doped LC rapidly transitioned to the optically transparent reentrant isotropic phase. No annealing was required. The capillaries were then heated back to room temperature to carry out X-ray diffraction in the reentrant isotropic phase, after which they were heated to the uniaxial nematic phase and cooled at −0.5 °C per minute to selected temperatures where X-ray diffraction measurements of the N and SmZ_A phases were carried out. In the EMIM/DIO mixtures, crystals of DIO typically started to appear when the sample was cooled to between 50 °C and 40 °C, making it challenging to obtain diffraction images of the N_F phase. The capillary could be reheated to the nematic and quenched to the I_R^{lam} phase as many times as desired.

The phase transition temperatures in cells and capillaries were determined using polarized light microscopy while cooling the samples at −0.5 °C per minute. DIO crystals typically started to nucleate and grow at around 40 °C in such temperature scans. In order to favor formation of the I_R^{lam} phase rather than the crystal, it is necessary to cool the samples more quickly, which prevents the crystal phase from growing to cover the whole volume before the transition to the I_R^{lam} phase can take place. For example, crystallization could be suppressed by cooling at −3 °C per minute, by which means a cell with the I_R^{lam} phase filling the entire volume could be obtained. In order to measure the precise temperature of the N_F – I_R^{lam} transition, the cell was first quenched to 30 °C and then cooled at −0.5 °C per minute to the transition at about 27 °C.

The I_R^{lam} phase in the DIO/EMIM mixtures is apparently less thermodynamically stable than the crystal. The crystal phase was typically observed to start nucleating following overnight storage at 20 °C. However, the I_R^{lam} phase was stable for at least five days if the sample was held at 9 °C. Upon heating at 0.5 °C per minute, the I_R^{lam} phase transitioned to the N_F phase at $T \sim$ 45 °C, after which the sample rapidly crystallized.

X-ray scattering

For SAXS and WAXS experiments, LC samples were filled into thin-wall capillaries 0.7 to 1 mm in diameter. Data presented here are powder averages obtained on cooling using a Forvis microfocus SAXS/WAXS system with a photon energy of CuK_α 8.04 keV (wavelength = 1.54 Å). Each X-ray exposure took ∼1 h at a given temperature.

This journal is © The Royal Society of Chemistry 2025

Open Access Article. Published on 06 Januar 2025. Downloaded on 09.05.26 05:53:12.
This article is licensed under a Creative Commons Attribution 3.0 Unported Licence.

Polarized light microscopy

Optical microscopy of LC cells viewed in transmission between crossed polarizer and analyzer, with such cells having the LC between uniformly spaced, surface-treated glass plates, provides key evidence for the macroscopic polar ordering, uniaxial optical textures, and fluid layer structure in LC phases and enables direct visualization of the director field, $\boldsymbol{n}(\boldsymbol{r})$, and, apart from its sign, of $\boldsymbol{P}(\boldsymbol{r})$.

Electro-optics

For making electro-optical measurements, the mixtures were filled into planar-aligned, in-plane switching test cells (Instec, Inc.) with unidirectionally buffed alignment layers arranged antiparallel on the two plates, which were uniformly spaced 3.5 μm apart. In-plane ITO electrodes on one of the plates were spaced by a 1 mm wide gap and the buffing was along a direction rotated 3° from parallel to the electrode edges. Such surfaces give a quadrupolar alignment of the N and SmZ_A directors along the buffing axis and polar alignment of the N_F at each plate, leading to a director/polarization field in the N_F phase that is parallel to the plates and has a π twist between the cell surfaces.[8]

Author contributions

B. Z., M. S., X. C., V. M., N. A. C. designed and conducted experiments and analyzed data. B. Z., M. S., X. C., N. A. C. interpreted the results. E. K. and D. M. W. synthesized materials. N. A. C., B. Z., J. E. M. wrote and edited the manuscript. M. A. G., J. E. M., N. A. C. supervised research.

Data availability

The data supporting this article have been included in the ESI.†

Conflicts of interest

In accordance with University of Colorado policy and our ethical obligations as researchers, we are reporting that several authors have a financial interest in a company (Polaris Electro-Optics, Inc.) that may be affected by the research reported in this paper. We have disclosed those interests fully to the University of Colorado and have in place an approved plan for managing any potential conflicts arising from that involvement.

Acknowledgements

This work was supported by NSF Condensed Matter Physics Grants DMR-1710711 and DMR-2005170, by NSF Materials Research Science and Engineering Centers (MRSEC) Grant DMR-1420736, by the State of Colorado OEDIT Grant APP-354288, and by a grant from Polaris Electro-Optics. X-ray experiments were performed in the Materials Research X-ray Diffraction Facility at the University of Colorado Boulder (RRID: SCR_019304), with instrumentation supported by NSF MRSEC Grant DMR-1420736.

References

1 R. J. Mandle, S. J. Cowling and J. W. Goodby, *Phys. Chem. Chem. Phys.*, 2017, **19**, 11429–11435, DOI: 10.1039/C7CP00456G.
2 A. Mertelj, L. Cmok, N. Sebastián, R. J. Mandle, R. R. Parker, A. C. Whitwood, J. W. Goodby and M. Čopič, *Phys. Rev. X*, 2018, **8**, 041025, DOI: 10.1103/PhysRevX.8.041025.
3 N. Sebastian, L. Cmok, R. J. Mandle, M. R. de la Fuente, I. Drevenšek Olenik, M. Čopič and A. Mertelj, *Phys. Rev. Lett.*, 2020, **124**, 037801, DOI: 10.1103/PhysRevLett.124.037801.
4 H. Nishikawa, K. Shiroshita, H. Higuchi, Y. Okumura, Y. Haseba, S. Yamamoto, K. Sago and H. Kikuchi, *Adv. Mater.*, 2017, **29**, 1702354, DOI: 10.1002/adma.201702354.
5 X. Chen, E. Korblova, D. Dong, X. Wei, R. Shao, L. Radzihovsky, M. A. Glaser, J. E. Maclennan, D. Bedrov, D. M. Walba and N. A. Clark, *Proc. Natl. Acad. Sci. U. S. A.*, 2020, **117**, 14021–14031, DOI: 10.1073/pnas.2002290117.
6 J. Li, H. Nishikawa, J. Kougo, J. Zhou, S. Dai, W. Tang, X. Zhao, Y. Hisai, M. Huang and S. Aya, *Sci. Adv.*, 2021, **7**, eabf5047, DOI: 10.1126/sciadv.abf5047.
7 X. Chen, Z. Zhu, M. J. Magrini, E. Korblova, C. S. Park, M. A. Glaser, J. E. Maclennan, D. M. Walba and N. A. Clark, *Liq. Cryst.*, 2022, **49**, 1531–1544, DOI: 10.1080/02678292.2022.2058101.
8 X. Chen, E. Korblova, M. A. Glaser, J. E. Maclennan, D. M. Walba and N. A. Clark, *Proc. Natl. Acad. Sci. U. S. A.*, 2021, **118**, e2104092118, DOI: 10.1073/pnas.2104092118.
9 X. Chen, E. Korblova, M. A. Glaser, J. E. Maclennan, D. M. Walba and N. A. Clark, Polar in-plane surface orientation of a ferroelectric nematic liquid crystal: polar monodomains and twisted state electro-optics, *arXiv*, 2020, preprint, arXiv:2012.15335, DOI: 10.48550/arXiv.2012.15335.
10 H. Nishikawa and F. Araoka, A New Class of Chiral Nematic Phase with Helical Polar Order, *Adv. Mater.*, 2021, **33**, 2101305, DOI: 10.1002/adma.202101305.
11 X. Zhao, J. Zhou, H. Nishikawa, J. Li, J. Kougo, Z. Wan, M. Huang and S. Aya, Observation of Spontaneous Helielectric Nematic Fluids: Electric Analogy to Helimagnets, *Proc. Natl. Acad. Sci. U. S. A.*, 2021, **118**, e2111101118, DOI: 10.1073/pnas.2111101118.
12 C. Feng, R. Saha, E. Korblova, D. M. Walba, S. N. Sprunt and A. Jákli, Electrically Tunable Reflection Color of Chiral Ferroelectric Nematic Liquid Crystals, *Adv. Opt. Mater.*, 2021, **9**, 2101230, DOI: 10.1002/adom.202101230.
13 X. Chen, V. Martinez, E. Korblova, G. Freychet, M. Zhernenkov, M. A. Glaser, C. Wang, C. Zhu, L. Radzihovsky, J. E. Maclennan, D. M. Walba and N. A. Clark, *Proc. Natl. Acad. Sci. U. S. A.*, 2023, **120**, e2217150120, DOI: 10.1073/pnas.2217150120.
14 X. Chen, V. Martinez, P. Nacke, E. Korblova, A. Manabe, M. Klasen-Memmer, G. Freychet, M. Zhernenkov, M. A. Glaser, L. Radzihovsky, J. E. Maclennan, D. M. Walba, M. Bremer, F. Giesselmann and N. A. Clark, *Proc. Natl. Acad. Sci. U. S. A.*, 2022, **119**, e2210062119, DOI: 10.1073/pnas.2210062119.
15 H. Kikuchi, H. Matsukizono, K. Iwamatsu, S. Endo, S. Anan and Y. Okumura, *Adv. Sci.*, 2022, **9**, 2202048, DOI: 10.1002/advs.202202048.
16 X. Chen, M. Shuai, B. Zhong, V. Martinez, E. Korblova, M. A. Glaser, J. E. Maclennan, D. M. Walba and

Open Access Article. Published on 06 Januar 2025. Downloaded on 09.05.26 05:53:12.
This article is licensed under a Creative Commons Attribution 3.0 Unported Licence.

N. A. Clark, *Thermotropic reentrant isotropy and induced antiferroelectricity in the ferroelectric nematic material RM734*. *arXiv*, 2023, preprint, arXiv: 2309.04935, DOI: 10.48550/arXiv.2309.04935.

17 B. Zhong, M. Shuai, X. Chen, V. Martinez, E. Korblova, M. A. Glaser, J. E. Maclennan, D. M. Walba and N. A. Clark, Thermotropic reentrant isotropy and induced antiferroelectricity in the ferroelectric nematic realm: Comparing RM734 and DIO, *arXiv*, 2023, preprint, arXiv:2312.17400, DOI: 10.48550/arXiv.2312.17400.

18 M. E. Fisher, An infinity of commensurate phases in a simple Ising system: The ANNNI model, *J. Appl. Phys.*, 1981, **52**, 2014–2018, DOI: 10.1063/1.329598.

19 A. Aharony, Critical behavior of magnets with dipolar interactions. V. Uniaxial magnets in d-dimensions, *Phys. Rev. B*, 1973, **8**, 3363–3370, DOI: 10.1103/PhysRevB.8.3363.

20 K. DeBell, A. B. MacIsaac and J. P. Whitehead, Dipolar effects in magnetic thin films and quasi-two-dimensional systems, *Rev. Mod. Phys.*, 2000, **72**, 225–257, DOI: 10.1103/RevModPhys.72.225.

21 H. Sun, H. Orihara and Y. Ishibashi, A Phenomenological Theory of Ferroelectric and Antiferroelectric Liquid Crystals Based on a Discrete Model, *J. Phys. Soc. Jpn.*, 1993, **62**, 2706–2718, DOI: 10.1143/JPSJ.62.2706.

22 Y. Song, M. Deng, Z. Wang, J. Li, H. Lei, Z. Wan, R. Xia, S. Aya and M. Huang, *J. Phys. Chem. Lett.*, 2022, **13**, 9983–9990, DOI: 10.1021/acs.jpclett.2c02846.

23 N. A. Clark and R. B. Meyer, Strain-induced instability of monodomain smectic A and cholesteric liquid-crystals, *Appl. Phys. Lett.*, 1973, **22**, 493–494, DOI: 10.1063/1.1654481.

24 N. A. Clark, T. P. Rieker and J. E. Maclennan, Director and layer structure of SSFLC cells, *Ferroelectrics*, 1988, **85**, 79–97, DOI: 10.1080/00150198808007647.

25 S. T. Lagerwall, *Ferroelectric and antiferroelectric liquid crystals*, Wiley VCH, Weinheim, 1999, ISBN 3-527-2983 1-2.

26 V. Luzzati and P. A. Spegt, Polymorphism of lipids, *Nature*, 1967, **215**, 701–704, DOI: 10.1038/215701a0.

27 P. A. Spegt and P. A. Skoulios, Structure des Savons de Strontium en Fonction de la Température, *Acta Crystallogr.*, 1966, **21**, 892–897, DOI: 10.1107/S0365110X66004158.

28 G. W. Gray, B. Jones and J. Marson, Mesomorphism and Chemical Constitution. Part VII. The effect of 3′-substituents on the mesomorphism of the 4′-*n*-alkoxydiphenyl-4-carboxylic acids and their alkyl esters, *J. Chem. Soc.*, 1957, 393–401, DOI: 10.1039/JR9570000393.

29 G. Etherington, A. J. Leadbetter, X. J. Wang, G. W. Gray and A. Tajbakhsh, Structure of the smectic D phase, *Liq. Cryst.*, 1986, **1**, 209–214, DOI: 10.1080/02678298608086509.

30 D. Guillon and A. Skoulios, Molecular model for the ''smectic D'' mesophase, *Europhys. Lett.*, 1987, **3**, 79–85, DOI: 10.1209/0295-5075/3/1/013.

31 S. Kutsumizu, The thermotropic cubic phase: a curious mesophase, *Curr. Opin. Solid State Mater. Sci.*, 2002, **6**, 537–543, DOI: 10.1016/S1359-0286(03)00008-1.

32 M. Imperor-Clerc, Thermotropic cubic mesophases, *Curr. Opin. Colloid Interface Sci.*, 2005, **9**, 370–376, DOI: 10.1016/j.cocis.2004.12.004.

33 C. Tschierske, Mirror symmetry breaking in liquids and liquid crystals, *Liq. Cryst.*, 2018, **45**, 2221–2252, DOI: 10.1080/02678292.2018.1501822.

34 J. Seddon, Structural studies of liquid crystals by x-ray diffraction, in *Handbook of Liquid Crystals*, ed., D. Demus, J. Goodby, G. W. Gray, H.-W. Spiess and V. Vill, Wiley VCH, 2008, vol. 1, p. 641.

35 H. Schubert, J. Hauschild, D. Demus and S. Hoffmann, Diacylhydrazin-Mesogene; Symmetrische 1,2-Dibenzoylhydrazinderivate, *Z. Chem.*, 1978, **18**, 256, DOI: 10.1002/zfch.19780180706.

36 D. Demus, A. Gloza, H. Hartung and A. Hauser, New thermotropic cubic mesophases, *Cryst. Res. Technol.*, 1981, **16**, 1445–1451, DOI: 10.1002/crat.19810161225.

37 Y. Maeda, S. Kutsumizu and S. Sakurai, The pressure effect on thermotropic cubic phases of 1,2-bis(4′-*n*-alkoxybenzoyl)-hydrazines, *Phys. Chem. Chem. Phys.*, 2014, **16**, 4329–4337, DOI: 10.1039/C3CP54471K.

38 S. Kutsumizu, H. Mori, M. Fukatami, S. Naito, K. Sakajiri and K. Saito, Cubic phase formation and interplay between alkyl chains and hydrogen bonds in 1,2-bis(4′-*n*-alkoxybenzoyl)hydrazines (BABH-*n*), *Chem. Mater.*, 2008, **20**, 3675–3687, DOI: 10.1021/cm703684v.

39 Y. Yasuhisa, Y. Nakazawa, S. Kutsumizu and S. Kazuya, Molecular packing in two bicontinuous Ia3d gyroid phases of calamitic cubic mesogens BABH(*n*): roles in structural stability and reentrant behavior, *Phys. Chem. Chem. Phys.*, 2019, **21**, 23705–23712, DOI: 10.1039/C9CP04424H.

40 S. Kutsumizu, H. Mori, M. Fukatami, S. Naito, K. Sakajiri and K. Saito, Cubic Phase Formation and Interplay between Alkyl Chains and Hydrogen Bonds in 1,2-Bis(4′-*n*-alkoxybenzoyl)hydrazines (BABH-*n*), *Chem. Mater.*, 2008, **20**, 3675–3687, DOI: 10.1021/cm703684v.

41 K. Saito, T. Shinhara, T. Nakamoto, S. Kutsumizu, S. Yano and M. Sorai, Degree of disorder in cubic mesophases in thermotropics: Thermodynamic study of a liquid crystal showing two cubic mesophases, *Phys. Rev. E:Stat., Nonlinear, Soft Matter Phys.*, 2002, **65**, 031719, DOI: 10.1103/PhysRevE.65.031719.

42 Y. Nakazawa, Y. Yamamura, S. Kutsumizu and K. Saito, Molecular Mechanism responsible for reentrance to Ia3d gyroid phase in cubic mesogen BABH(*n*), *J. Phys. Soc. Jpn.*, 2012, **81**, 094601, DOI: 10.1143/JPSJ.81.094601.

43 K. Saito and M. Sorai, Quasi-binary picture of thermotropic liquid crystals and its application to cubic mesophases, *Chem. Phys. Lett.*, 2002, **366**, 56–61, DOI: 10.1016/S0009-2614(02)01535-X.

44 S. Kutsumizu, K. Akane, Y. Yasuhisa, T. Udagawa, T. Otaki, M. Masuda, M. Yohei and K. Saito, Stabilization of bicontinuous cubic phase and its two-sided nature produced by use of siloxane tails and introduction of molecular nonsymmetry, *Chem. – Eur. J.*, 2021, **27**, 10293–10302, DOI: 10.1002/chem.202101233.

45 M. Yoneya, Toward rational design of complex nanostructured liquid crystals, *Chem. Rec.*, 2011, **11**, 66–76, DOI: 10.1002/tcr.201000025.

This journal is © The Royal Society of Chemistry 2025

Open Access Article. Published on 06 Januar 2025. Downloaded on 09.05.26 05:53:12.
This article is licensed under a Creative Commons Attribution 3.0 Unported Licence.

46 J. M. Seddon and R. H. Templer, in Polymorphism of lipid-water systems, ed. R. Lipowsky, E. Sackmann, *Handbook of Biological Physics*, Elsevier, 1995, pp. 97–160.
47 L. E. Hough, M. Spannuth, M. Nakata, D. A. Coleman, C. D. Jones, G. Dantlgraber, C. Tschierske, J. Watanabe, E. Körblova, D. M. Walba, J. E. Maclennan, M. A. Glaser and N. A. Clark, Chiral isotropic liquids from achiral molecules, *Science*, 2009, **325**, 452–456, DOI: **10.1126/science.1170028**.
48 C. Dressel, T. Reppe, S. Poppe, M. Prehm, H. Lu, X. Zeng, G. Ungar and C. Tschierske, Helical Networks of π-Conjugated Rods – A Robust Design Concept for Bicontinuous Cubic Liquid Crystalline Phases with Achiral Ia$\bar{3}$d and Chiral I23 lattice, *Adv. Func. Mat*, 2020, **30**, 2004353, DOI: **10.1002/adfm.202004353**.
49 C. Tschierske and G. Ungar, Mirror symmetry breaking by chirality synchronisation in liquids and liquid crystals of achiral molecules, *ChemPhysChem*, 2015, **17**, 9–26, DOI: **10.1002/cphc.201500601**.
50 H. Nádasi, C. Lischka, W. Weissflog, I. Wirth, S. Diele, G. Pelzl and H. Kresse, *Mol. Cryst. Liq. Cryst.*, 2003, **399**, 69–84, DOI: **10.1080/15421400390225471**.
51 D. Chen, Y. Shen, J. Aguero, E. Korblova, D. M. Walba, N. Kapernaum, F. Giesselmann, J. Watanabe, J. E. Maclennan, M. A. Glaser and N. A. Clark, *ChemPhysChem*, 2014, **15**, 1502–1507, DOI: **10.1002/cphc.201300912**.
52 J. V. Selinger, *Annu. Rev. Condens. Matter Phys.*, 2022, **13**, 49–71, DOI: **10.1146/annurev-conmatphys-031620-105712**.
53 J. G. Fernsler, M. A. Glaser, R. F. Shao, D. A. Coleman, J. E. Maclennan, D. R. Link, C. Chang, K. Lanham, D. M. Walba, C. Boyer, J. A. Zasadzinski and N. A. Clark, *Liq. Cryst.*, 2017, **44**, 769–783, DOI: **10.1080/02678292.2016.1240835**.
54 P. J. Ackerman, J. van de Lagemaat and I. I. Smalyukh, Self-assembly and electrostriction of arrays and chains of hopfion particles in chiral liquid crystals, *Nat. Commun.*, 2015, **6**, 6012, DOI: **10.1038/ncomms7012**.
55 J. S. B. Tai and I. I. Smalyukh, Three-dimensional crystals of adaptive knots, *Science*, 2019, **365**, 1449–1453, DOI: **10.1126/science.aay163**.
56 Y. Y. Mai and A. Eisenberg, Self-assembly of block copolymers, *Chem. Soc. Rev.*, 2012, **41**, 5969–5985, DOI: **10.1039/C2CS35115C**.
57 J. Yamamoto and H. Tanaka, Transparent nematic phase in a liquid-crystal-based microemulsion, *Nature*, 2001, **409**, 321–325, DOI: **10.1038/35053035**.
58 M. Caggioni, A. Giacometti, T. Bellini, N. A. Clark, F. Mantegazza and A. Maritan, Pretranslational behavior of a water in liquid crystal microemulsion close to the demixing transition: evidence for intermicellar attraction mediated by paranematic fluctuations, *J. Chem. Phys.*, 2005, **122**, 214721, DOI: **10.1063/1.1913444**.
59 G. A. Hinshaw, Jr., R. G. Petschek and R. A. Pelcovits, Modulated phases in thin ferroelectric liquid-crystal films, *Phys. Rev. Lett.*, 1988, **60**, 1864–1867, DOI: **10.1103/PhysRevLett.60.1864**.
60 G. A. Hinshaw, Jr. and R. G. Petschek, Transitions and modulated phases in centrosymmetric ferroelectrics, *Phys. Rev. B: Condens. Matter Mater. Phys.*, 1988, **37**, 2133–2155, DOI: **10.1103/PhysRevA.39.5914**.
61 S. M. Shamid, D. W. Allender and J. V. Selinger, Predicting a polar analog of chiral blue phases in liquid crystals, *Phys. Rev. Lett.*, 2014, **113**, 237801, DOI: **10.1103/PhysRevLett.113.237801**.
62 M. P. Rosseto and J. V. Selinger, Theory of the splay nematic phase: Single versus double splay, *Phys. Rev. E*, 2020, **101**, 052707, DOI: **10.1103/PhysRevE.101.052707**.
63 R. Hayes, G. G. Warr and R. Atkin, Structure and Nanostructure in Ionic Liquids, *Chem. Rev.*, 2015, **115**, 6357–6426, DOI: **10.1021/cr500411q**.